



Experimental and numerical investigation of building effects on wind erosion of a granular material stockpile

Maria Clara S. Ferreira¹ · Bruno Furieri² · Cristina L. de Moraes² · Jamily F. Stocco² · Neyval C. Reis Jr² · Jean-Luc Harion³ · Jane Meri Santos²

Received: 25 September 2019 / Accepted: 20 July 2020 / Published online: 20 August 2020
© Springer-Verlag GmbH Germany, part of Springer Nature 2020

Abstract

In the present work, wind tunnel experiments and numerical simulations were carried out to evaluate the physical behaviour of the fluid flow of a stockpile in the presence of an isolated cubic building. Comparing the obtained experimental results with those for the isolated stockpile configuration and observing the differences in the erosion patterns and emission estimates was possible to conclude that (i) the emissions considerably increase due to the presence of the building; (ii) the higher the free stream velocity, due to the presence of the obstacle, the more efficient the dynamics of the pavement process; and (iii) the increase of the gap between the building and the pile does not generate expressive changes in the emitted mass measurements. These findings play an important role since it is possible to obtain an optimal industrial open yard configuration where fewer particles are emitted to the atmosphere.

Keywords Air pollution · Particulate emission control · Industrial site arrangement · Wind tunnel · CFD · Turbulent flows

Introduction

Wind erosion process can lead to several environmental consequences as desertification, land degradation, loss of material and increase of particulate concentrations to the atmosphere. The air pollution is of particular interest since it has a direct impact on human health, mainly in regions with high availability of diffuse sources such as ore and coal stored in piles on open yards of industrial units.

Wind erosion is dominated by the aerodynamic forces (drag and lift forces) that act to remove the particle from the surface and by the gravity and cohesion forces that act to

restrain its movement. The aerodynamic forces are usually quantified by means of the friction velocity, u_* (square root of the ratio between wall shear stress and density), a variable characteristic of the boundary layer flow that represents the conceptual value of shear stress, τ , on the surface. The gravity and cohesion forces are considered by the threshold friction velocity (u_{*t}), which defines the minimum friction velocity in which particle movement is initiated (Shao 2008). The balance between the friction velocity and the threshold friction velocity determines a criterion (Bagnold 1941; Iversen and White 1982; Foucaut and Stanislas 1996; Shao and Lu 2000) that is used to verify if particles will take-off. If the wind friction velocity is greater than the particles threshold friction velocity ($u_* > u_{*t}$), the particles will move. These particles are known as erodible for the referred wind flow velocity. Otherwise, if the friction velocity does not trespass the threshold value ($u_* < u_{*t}$), they will be called non-erodible and they will not take-off. A very common take-off criterion used is from (Shao and Lu 2000):

$$u_{*t} = 0.11 \sqrt{\frac{\rho_p - \rho}{\rho} g D + \frac{\gamma}{\rho D}} \quad (1)$$

Responsible Editor: Philippe Garrigues

✉ Bruno Furieri
bruno.furieri@ufes.br

¹ Department of Mathematics, Instituto Federal do Espírito Santo, 29056-255 Vitória, ES, Brazil

² Environmental Engineering Department, Universidade Federal do Espírito Santo, 29060-970 Vitória, ES, Brazil

³ IMT Lille-Douai, F-59500 Douai, France

where ρ is the air density (kg/m^3), ρ_p is the particle density (kg/m^3), D is the particle diameter (m), g is the acceleration due to gravity (m/s^2) and γ is a parameter called surface energy that characterises cohesion (kg/s^2).

It is important to discuss that u_{*t} is related to the material and surface of agglomeration properties, such as texture, moisture, density of the material and particle size distribution, while u_* is related to surface aerodynamic properties and atmospheric flow conditions (Shao 2008). However, specific scenarios in the context of industrial open yards can also influence these properties, as stockpiles geometries and structures in the surroundings, as equipments, buildings and even other stockpiles.

Caliman (2017) and de Moraes et al. (2018) have shown that the inclined surface of the stockpile causes a strong influence on the gravity force and consequently on the threshold friction velocity. Based on the angle, θ , at which the fluid flows over the surface, the threshold friction velocity is modified. If the flow is ascending on the stockpile surface, it is against the gravity force causing an increase in particle threshold friction velocity being harder to emit. If the flow is descending on the stockpile surface, the shear stress is in the same direction of the gravity force causing a decrease in threshold friction velocity being easier to emit. The angle θ (Caliman 2017) and its influence in the threshold friction velocity (Iversen and Rasmussen 1994) are given by the following relations:

$$\theta = \arcsin(\tau_z/\tau) \quad (2)$$

where τ_z (Pa) is the vertical component of the shear stress.

$$\frac{u_{*t}(\theta)^2}{u_{*t}(0)^2} = \cos \theta + \frac{\sin \theta}{\tan \xi} \quad (3)$$

where ξ is the internal friction angle. The $u_{*t}(0)$ refers to the threshold friction velocity of a particle on a bed. $u_{*t}(0)$ can be obtained through several techniques, as wind tunnel tests or sieving.

Turpin and Harion (2010), Ferreira and Fino (2012), Ferreira et al. (2013) and Furieri et al. (2012a, b) have shown that the surroundings can influence the shear stress distribution patterns over the stockpile surface causing an increase on the emitted mass depending on the distance and position of the obstacle next to the pile in relation to the incoming flow.

Turpin and Harion (2010) performed numerical simulations of a fully industrial site that was composed by buildings and stockpiles. Four main wind flow directions were tested in relation to the longitudinal side of the stockpiles. The stockpiles were 10 m high and the two groups of buildings considered had the mean height of the 90 m and 30 m. The authors showed that the buildings behave as huge obstacles for the wind flow and largely modify the flow structures over stockpiles mainly for the orientations of 90°

and 45°. According to emission estimates, it can increase up to 1525% with the presence of buildings for these wind flow orientations.

Ferreira and Fino (2012) proposed to study, through wind tunnel experiments, the erosion that occurs when two stockpiles are placed in tandem. The piles had 60 mm high (H) and two lengths were tested, $L=5H$ and $L=6H$. Two upstream velocities, 8.3 and 9.1 m/s, and two distances between the piles, $D=0$ and $D=H$, were tested. The results showed that for the lowest tested velocity the upstream pile remains practically unchanged and the downstream pile is considerably eroded. On the other hand, for the largest tested velocity, it was observed the entire erosion of the downwind pile. Finally, when the distance between the piles was analysed, the results showed that for distance $D=H$, the erosion is less compared with the distance $D=0$. It seems that small distances result in a more eroded downwind pile probably due the recirculation bubble generated between both piles. Ferreira et al. (2013) performed wind tunnel experiments similar to Ferreira and Fino (2012). Numerical simulations validated by the experimental work were carried out to complement the study. Detailed results were obtained by numerical simulations and the recirculation bubble between the piles was confirmed.

Furieri et al. (2012a, b) performed numerical simulations in order to compare the emission of an isolated stockpile and two parallel stockpiles. The stockpiles were oriented 60° to the main flow and two gaps between them were tested, 1e and 2e (where e is equal 0.894 times the stockpile height). In all cases were considered the upstream velocity of 6.5 m/s. The numerical results showed that an isolated stockpile emits less dust than when each stockpile is placed next to another. The protection effect pointed out by other authors (Cong et al. 2012; Diego and et al 2009) was not observed for this type of stockpile configuration.

Despite the use of numerical simulations being very useful to obtain more detailed results of the shear stress distribution over the stockpile surface (Badr and Harion 2005; 2007; Torano and et al 2007; Diego and et al 2009; Turpin and Harion 2009; Faria and et al 2011; Farimani et al. 2011; Furieri et al. 2012a; Derakhshani et al. 2013), except by the study of Ferreira and Fino (2012), the studies cited in the present work about surroundings effects on stockpile emissions did not perform experimental work. Experimental simulations are an important tool to validate numerical simulations and better visualise the erosion evolution over the stockpile surface, since, numerically the stockpile surface has been considered as a smooth and rigid wall as a simplification.

Recently, several researches have been carried out both numerical (Fang and et al 2018; Hilton and Cleary 2013; Kim and et al 2017; Liu et al. 2018; Jeong and et al 2014; Novak and et al 2015; Romeo and et al 2017; Ferreira

et al. 2019; Liu et al. 2019) and experimental (field and laboratory) (Bachelet and et al 2018; Cong et al. 2016; Cong et al. 2013; Ferreira et al. 2019; Funk et al. 2019; George and et al 2017; Giunta 2020; Walter et al. 2016) approaches in order to evaluate dust emission and transport in the atmosphere. The present work has as main objective to understand the phenomena of granular material storage piles erosion through both techniques simultaneously. In addition, the major part of the variables and discussions presented was not found anywhere in the literature.

In the present work, wind tunnel experiments and numerical simulations were carried out to evaluate the physical behaviour of the fluid flow interacting with stockpiles and to quantify the emission of a stockpile in the presence of an isolated cubic building. The orientation of the building to the main flow, the free stream velocities and the distance between the building and the pile were investigated. In order to better represent the reality, the experiments were performed with a mixture of erodible and non-erodible particles, since the non-erodible particles create low shear stress zones that also influence the emission not allowing the u_{*f} to be reached (Crawley and Nickling 2003; Furieri et al. 2013; Gillette and Stockton 1989; Gillies and et al 2015; Iversen et al. 1990; Marshall 1971; Marticorena and Bergametti 1995; Miri et al. 2017; Raupach and et al 1993; Tan and et al 2013; Leon Lyles and Schmeidler 2013; Raupach 1992; Turpin and Harion 2010).

Experimental study

The experimental work was performed in a wind tunnel, schematically presented in Fig. 1, with the following main dimensions: $H_s = 0.80$ m (height), $W_s = 1.50$ m (width)

and $L_s = 8.12$ m (length). The thickness of the boundary layer (δ) in the test section was sufficiently larger than the height of the stockpile h ($\delta = 16$ cm and $h = 7.7$ cm). Honeycombs and very fine grid were placed upstream and downstream the test section as an important function to break-up the great flow features coming from the inlet region and to prevent ventilator perturbations at outlet region. Besides that, multiple small cubic obstacles were set upstream of the test section in order to ensure the formation of a fully developed turbulent boundary layer. Moisture and temperature effects were not considered since the experiment was not performed in any extreme conditions of cold or hot weather. A photographic camera (Nikon D-100) was installed over the glass test section to register the evolution of wind erosion.

The stockpile models were formed inside the wind tunnel using a hopper and a mould (where the sand was discharged) with the same chosen volume and surface shape. The sand stockpile model was 7.7 cm high, 23.6 cm long and 57.9 cm wide with a 34.5° rest angle. Sand with density equal to $\rho_p = 2,630$ kg/m³ was used to compose a bimodal granulometry mixture with 80% of white sand (56.0 to 194.2 μ m) and 20% of black sand (700.0 to 1300.0 μ m). The colours of the sand allow the visualisation of high shear stress zones marked by accumulation of non-erodible particles, expected to be the black sand particles for all tested velocities based on Shao and Lu (2000) criterion.

Tests of repeatability for free stream velocity of 8 m/s were carried out to assure that the results obtained could be compared with each other. It was necessary to guarantee that (i) the initial mass of the stockpiles and (ii) the particle size distribution over the stockpiles surface had the same averaged value. The two types of sand were mixed up with a mixer and, after assembling the piles, measurements of

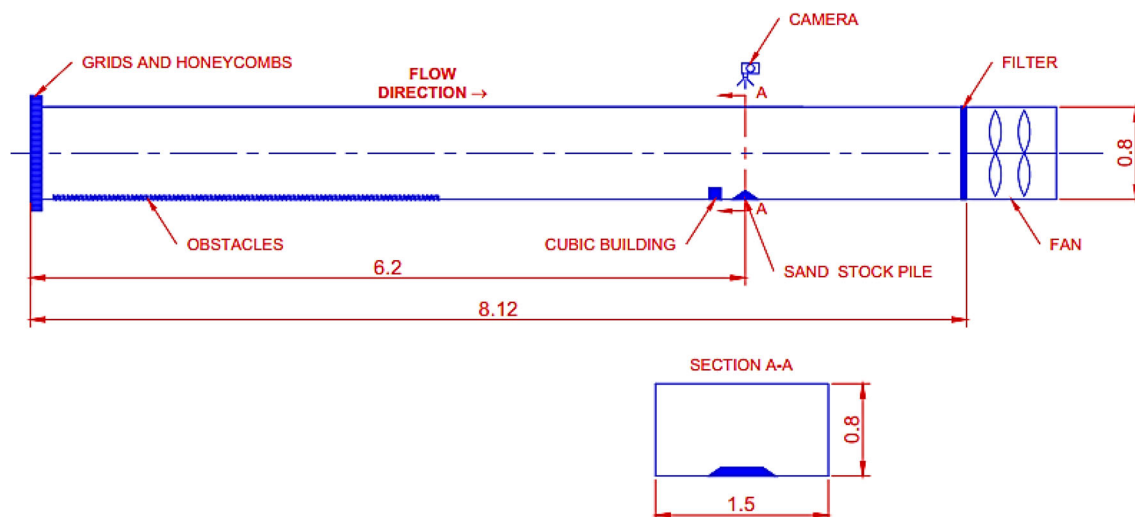


Fig. 1 Schema of wind tunnel experimental setup (the dimensions are in meters)

the initial and emitted mass were performed in triplicate. The results showed good agreement between the triple measurements, with averaged initial mass of 6190.0 g and averaged emitted mass of 325.53 g. The experimental emitted mass was obtained by the difference between the initial and final stockpile weights. The weighing device was the electronic balance BEL Engineering Mark K30.1 which has a resolution of 0.1 g.

The isolated cubic building was made by steel and its dimensions were chosen ($H_b = 10\text{cm}$) to obtain a cubic building higher than the stockpile. Photographs were taken at the beginning of the experiment and every 30 s up to 5 min. The last picture was taken after 15 min which no more emissions were observed, that is, the pavement of the pile surface was reached. The methodology of the experiments carried out is the same used in previous works. For more details, see the works of Furieri et al. (2012a), Furieri et al. (2013) and de Morais et al. (2018).

Three parameters were varied during the experiments: (i) distance between the building and the pile, with gaps of 0.5 and 1.5 times the cubic model height H_b ; (ii) orientation of the cube to the main flow, with angles of 90° (face-on) and 45° (edge-on) relative to the pile; and (iii) free stream velocities, 7, 8 and 9 m/s. Figure 2 shows a schematic view of the tested configurations.

It is important to clarify some aspects about similarity. All dimensions of the model are related to the corresponding dimensions in full scale by a constant scale factor (1:200). In the same way, the velocity direction and magnitude acting on the stockpile model may correspond to the same free

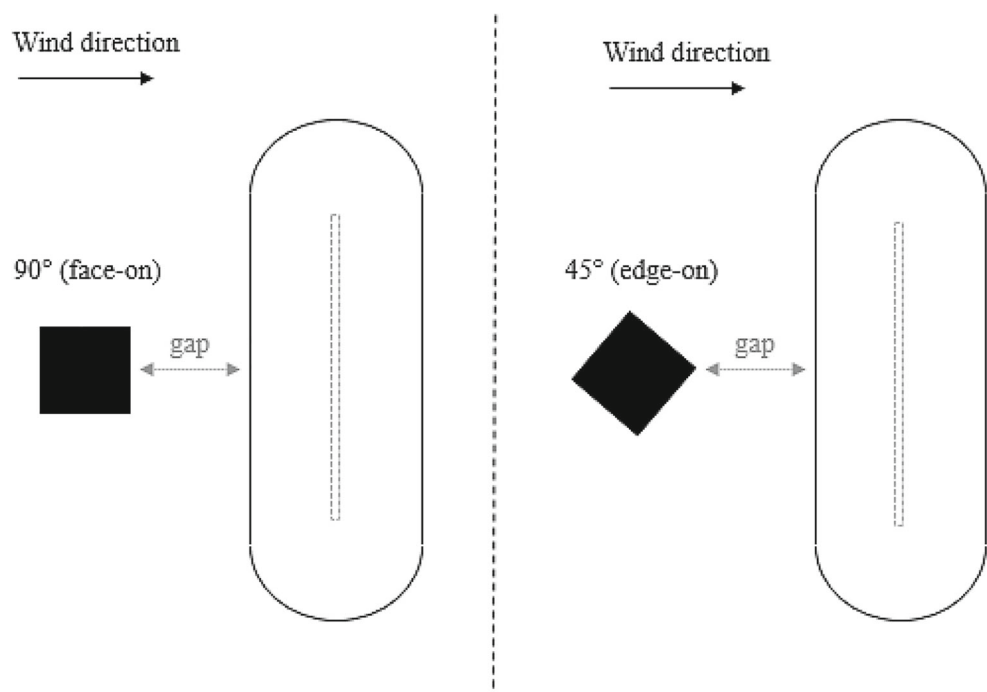
stream velocity value acting on the full scale stockpile. The Reynolds numbers are about 10^5 and 10^7 in wind tunnel and full scale, respectively. The Reynolds number of the experiments (10^5) reaches the independence criterion (above 10^4 according to Woodruff and Zingg (1953)), which would be enough to reach similarity between the model and the prototype (White 1996) for what we propose in the present work (Aliabadi 2018; Chew et al. 2018).

Numerical simulation setup

The numerical simulations were carried out in order to correctly simulate the experiments, except for the consideration of the pile as having a solid and smooth surface instead of roughness caused by the agglomeration of sand particles (a simplification imposed in the numerical model since the mesh should be greater than the roughness, what means do not respect the law of wall of the turbulence model). The numerical simulations were performed to provide the wall shear stress distribution on the pile surface and the flow pathlines, which could be associated to the erosion patterns observed in the experiments and even be input data to mathematical emission models (Caliman 2017; de Morais et al. 2018).

The three-dimensional equations of mass and momentum conservation were solved using the commercial software Ansys Fluent 15.0. Turbulence effects were accounted using the $k - \omega$ shear stress transport (SST) model (Menter 1994). The inlet boundary conditions for velocity

Fig. 2 Schema of the tested configurations. The dashed lines on the stockpile surface indicate the rounded crest



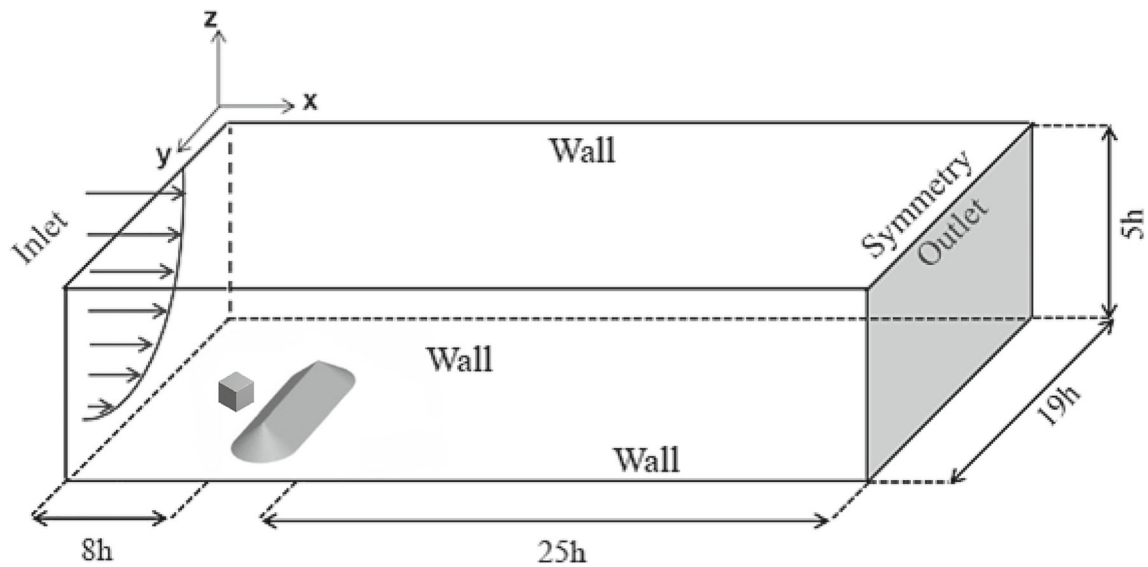


Fig. 3 Computational domain and boundary conditions. All the dimensions are scaled based on the stockpile height h (0.077 m)

(u , v and w), turbulent kinetic energy (k) and specific dissipation rate (ω) were obtained from previous numerical simulations (precursor empty domain) where a periodic streamwise flow was set to produce a fully developed channel flow. For the outlet boundary conditions, it was assumed that the flow is fully developed and all flow variables except pressure are assumed to have a zero normal gradient (outflow condition). For the upper boundary condition, symmetry was imposed, since only half of the wind tunnel height was simulated in order to reduce the computational costs. Symmetry condition implies that normal gradients of all variables are set to zero. Smooth walls with no-slip conditions are set at lateral domain walls, as well as, smooth walls at stockpile, cubic building and ground walls. All boundary conditions can be seen in Fig. 3.

The geometries and meshing were generated using the software Gambit. The mesh was built by extrusion from triangular cells defined on the ground surface and pile walls. The size of the first cell at the wall was taken as $z^+ \approx 4$ ($z^+ = \rho u_* z / \mu$), as required for the use of $k - \omega$ SST model ($z^+ \leq 5$) to ensure that no wall functions are used (for better accuracy) to account for the turbulence damping near walls. A mesh refinement near the walls is required due to the expected intense gradients close to these areas. All computational setup (modelling choices including meshing, turbulence closure and domain configurations) is based on previous validated numerical calculations performed by Badr and Harion (2005), Turpin (2010), Furieri et al. (2012a, 2013) and Caliman (2017). Details of the mesh in the stockpile and building surfaces are shown in Fig. 4 where it is possible to observe the refinement near the walls.

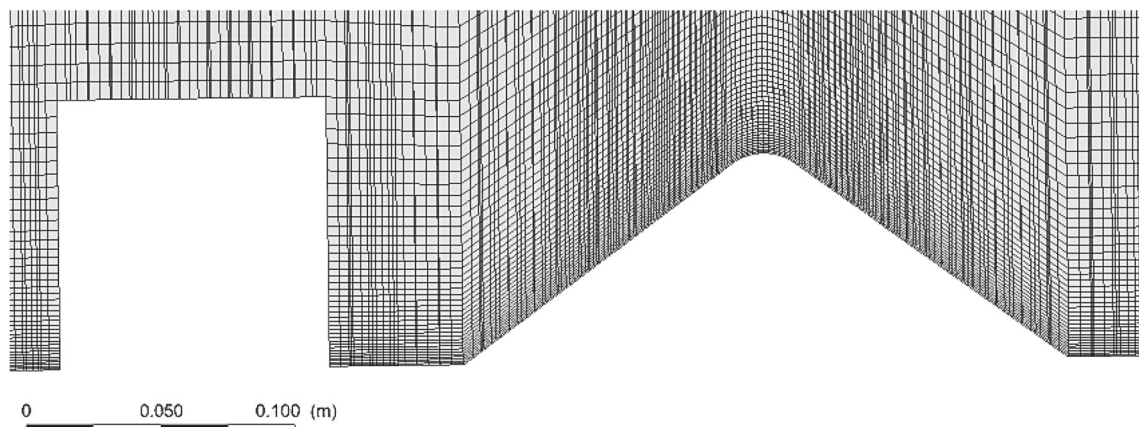


Fig. 4 Mesh construction with refinement near the walls

Results

Air flow and stockpile erosion patterns

Figures 5 and 6 show the photographs after the pavement phenomenon (a), the friction velocity distribution (b) and the pathlines (c) for a stockpile downstream a face-on cubic building and for a stockpile downstream an edge-on cubic building, respectively. Figure 7 shows the friction velocity distribution (a) and the photographs after the pavement phenomenon (b) for an isolated stockpile. The numerical results are presented in the dimensionless form ($u_*/u_{*,ref}$ and U/U_∞). The variable $u_{*,ref}$ is the friction velocity in a flat surface without influence of obstacles been equal to 0.34 m/s in this case. The variable U_∞ is the free stream velocity of 7 m/s. The calculation of u_* over the stockpile surface was based on the United States Environmental Protection Agency USEPA (2006) model for industrial wind erosion since the procedure considers the friction velocity over a rough surface. The friction velocity (m/s) is then estimated by:

$$u_* = 0.10u_{10}^+(u_s/u_r) \quad (4)$$

where u_{10}^+ is the fastest mile of reference anemometer for the period between disturbances (m/s), u_s is surface velocity measured at 25 cm from the full scale stockpile surface (m/s) (in the wind tunnel scale and numerical simulations this distance is equal 0.00125 cm) and u_r is the wind velocity (m/s) (details in USEPA 2006).

In Fig. 5, the large adverse pressure gradient upstream the cube promotes a deceleration of the fluid leading to a boundary layer separation and vortex shedding. As a consequence of the reverse flow behind the cube, there is an accumulation of sand in region R (see Fig. 5a), a zone characterised by low levels of shear (or friction velocity), as shown in Fig. 5b. Figure 5c shows the complex recirculation zone downstream of the cube, which clearly affects erosion on the windward wall of the pile. Therefore, in contrast with the configuration of an isolated stockpile (Fig. 7b), region A is strongly eroded for both tested gaps (specially for $0.5H_b$), which is consistent with the high levels of wall shear stress in this area. Also, an eroded zone B is noticeable for the gap $0.5H_b$ due to the stronger influence of the central vortex structure shown in Fig. 5c.

Figure 6 shows a much more intense bistable flow for this case, in which an asymmetrical pattern is detected in spite of the symmetrical geometry. The interaction between the pile and the cube also promotes an accumulation of sand in the zone R where shear stress is low. In addition, for this building orientation, it is possible to observe a more intense interaction between the vortices downstream the cube, leading the windward wall of the pile to be even more impacted as can be noticed by the greater accumulation of black particles (Fig. 6a). The leeward

wall of the pile, and also zone is more affected compared with the stockpile downstream an edge-on cubic building for both tested gaps. In an industrial site, it would be wise to avoid placing the piles near edge-on building position.

The comparison between u_* and u_{*t} can also be done to reinforce the discussion above. The threshold friction velocity for the sand used in the present work is equal to 0.25 m/s (Harion et al. 2010). Since $u_{*,ref}$ is equal to 0.34 m/s, it is possible to observe in Figs. 5b and 6b that the contours of $u_*/u_{*,ref}$ higher than 0.75 highlight regions where the friction velocity on the surface is greater than the threshold friction velocity. Thus, these would be the most eroded regions of the pile, which is confirmed by Figs. 5a and 6a. Furthermore, the friction velocity can be up to 2.5 times greater than the reference friction velocity (the high levels showed in Figs. 5b and 6b) leading us to evaluate the increased possibility of erosion occurs when the particles are arranged in structures such as stockpiles instead of a flat bed.

Another analysis can be made we consider the angle θ at which the fluid flows over the stockpile surface to calculate the threshold friction velocity according to Eq. 3. Figure 8a shows the distribution of the difference between the friction velocity and the modified threshold friction velocity over the stockpile surface for the case $0.5H_b$ at 7 m/s. The gray colour indicates regions where $(u_* - u_{*t}(\theta)) < 0$, that is, the friction velocity did not reach the particle threshold friction velocity value leading the particles to not take-off. The corresponding gray area of Fig. 8a in Fig. 8b shows that, indeed, no erosion was experimentally observed. The highlighted areas A, B, C and D represent regions where $(u_* - u_{*t}(\theta)) > 0$, that is, the friction velocity reaches the particle threshold friction velocity value leading the particle to take-off. The values of $(u_* - u_{*t}(\theta))$ which this occur are from 0.055 to 0.55 m/s if we take a look on Fig. 8a. Therefore, correct or reevaluate the threshold friction velocity would better explain the particle distribution over the stockpile surface when the USEPA model is used. In the final state of the wind erosion, this may be an interesting analysis that could be added to the USEPA methodology, mainly when the cases to be studied do not comprise those proposed by the agency.

For 8 m/s and 9 m/s cases, the same analysis is valid. Taking 8 m/s cases for a more detailed discussion, it is interesting to observe the phenomenon evolving over time. Figure 9 shows the temporal evolution of the wind erosion for 8 m/s upstream velocity when the cubic building is face-on and edge-on with a gap of $0.5H_b$. It is possible to observe that the effects of the flow are more intense and the erosion occurs faster when the stockpile is downstream an edge-on cubic building. At the same instant of time,

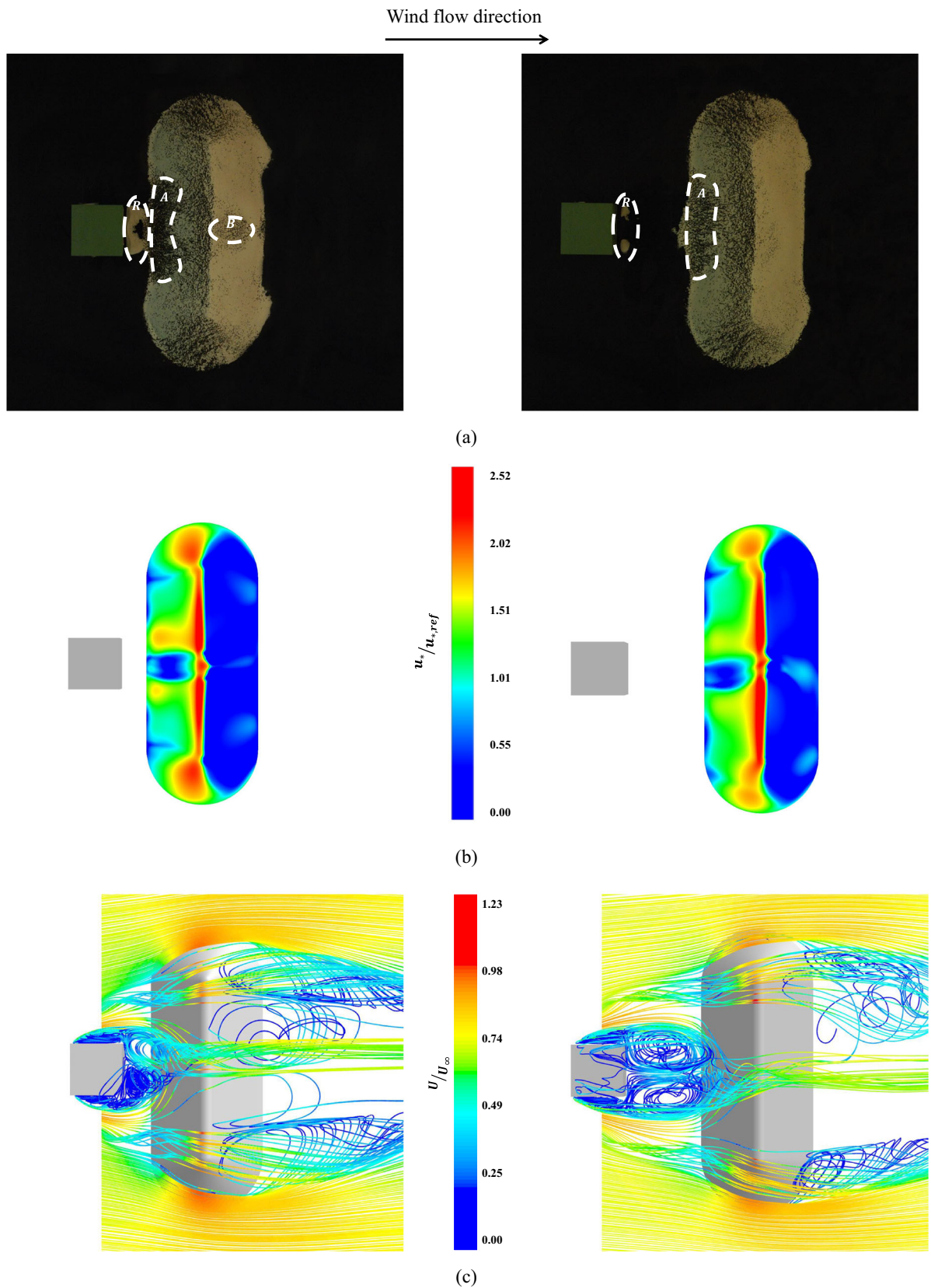


Fig. 5 Experimental and numerical results for a stockpile downstream face-on cubic building separated by gaps $0.5H_b$ and $1.5H_b$: **a** photograph of the top view of the eroded sand stockpile after pavement, **b**

friction velocity distribution on the pile surface and **c** pathlines of the flow over the pile. Highlighted are the regions R and B marked by low levels of shear stress and a vortex influence, respectively

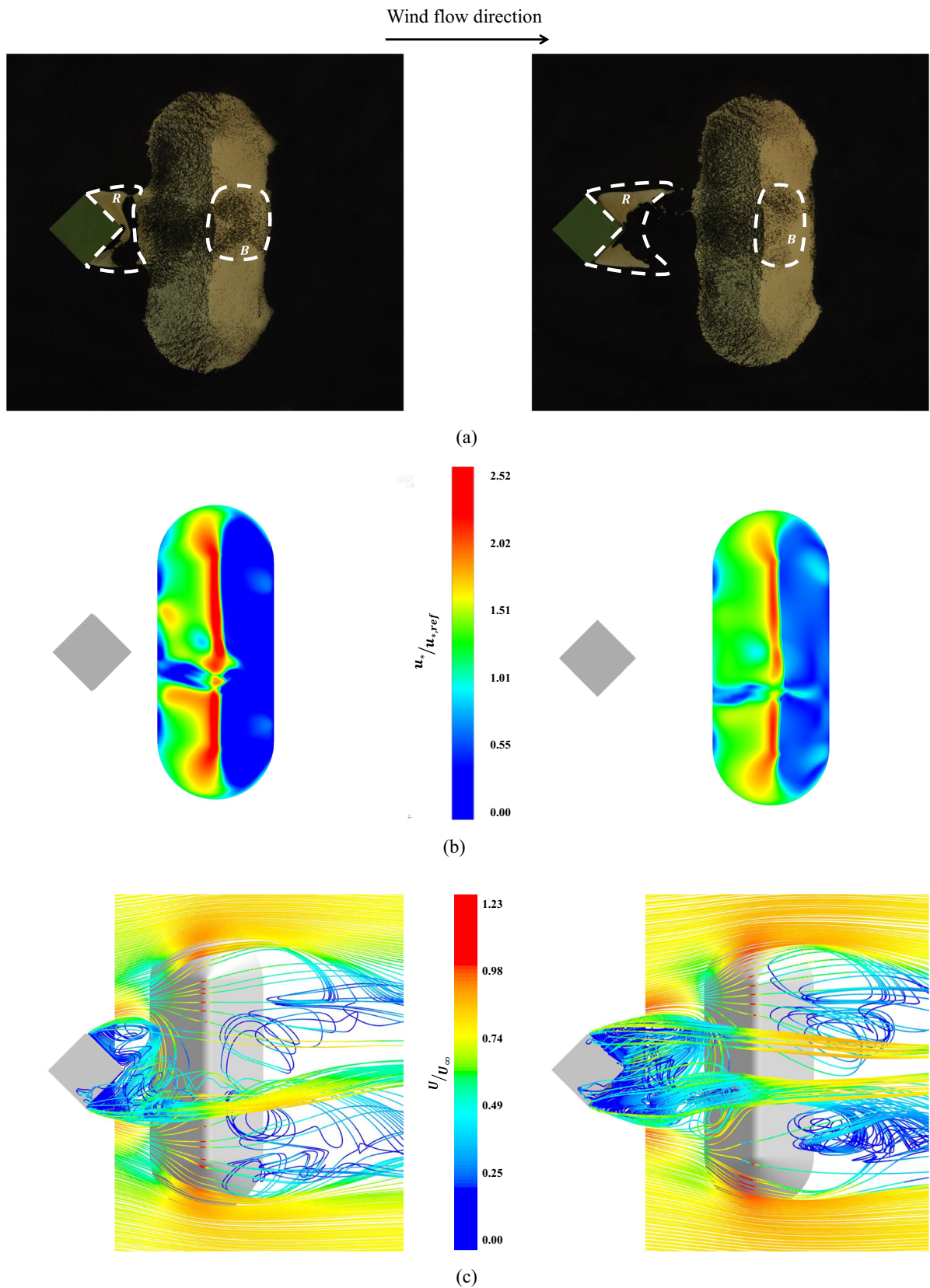


Fig. 6 Experimental and numerical results for a stockpile downstream edge-on cubic building separated by gaps $0.5H_b$ and $1.5H_b$: **a** photograph of the top view of the eroded sand stockpile after pavement, **b**

friction velocity distribution on the pile surface and **c** pathlines of the flow over the pile. Highlighted are the regions R and B marked by low levels of shear stress and a vortex influence, respectively

Fig. 7 Experimental and numerical results for an isolated stockpile for stream velocity of 7 m/s: **a** friction velocity distribution on the pile surface and **b** photograph of the top view of the eroded sand stockpile after pavement. Highlighted is region A, a very low shear stress zone when compared with the corresponding region in the case with the presence of an obstacle

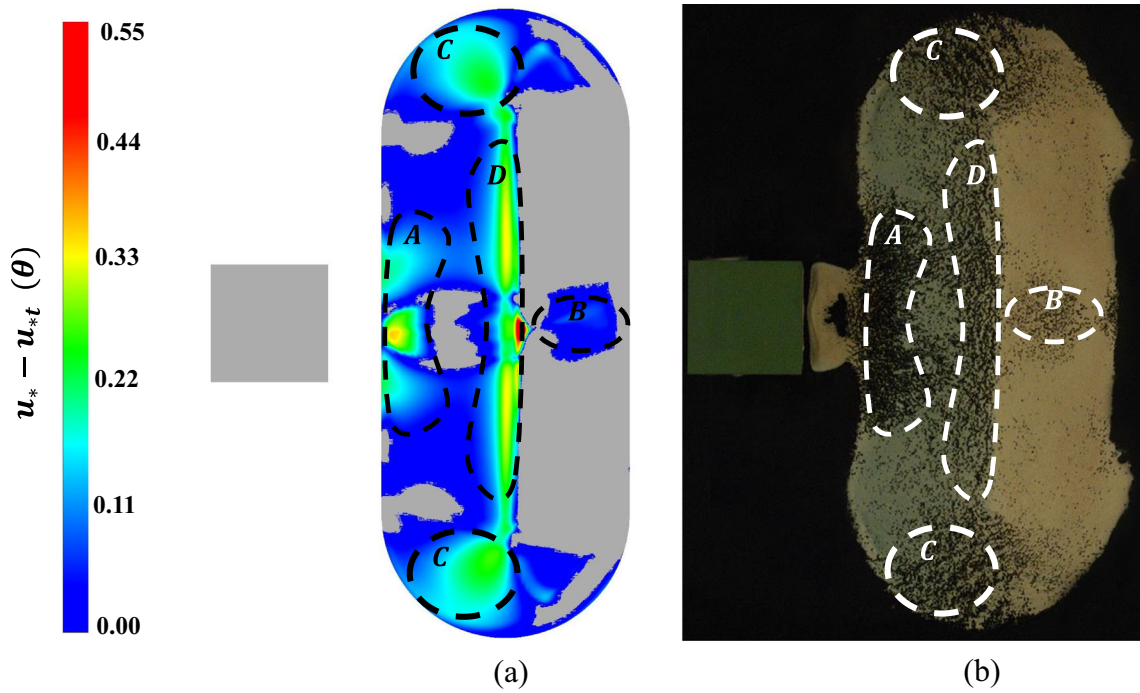
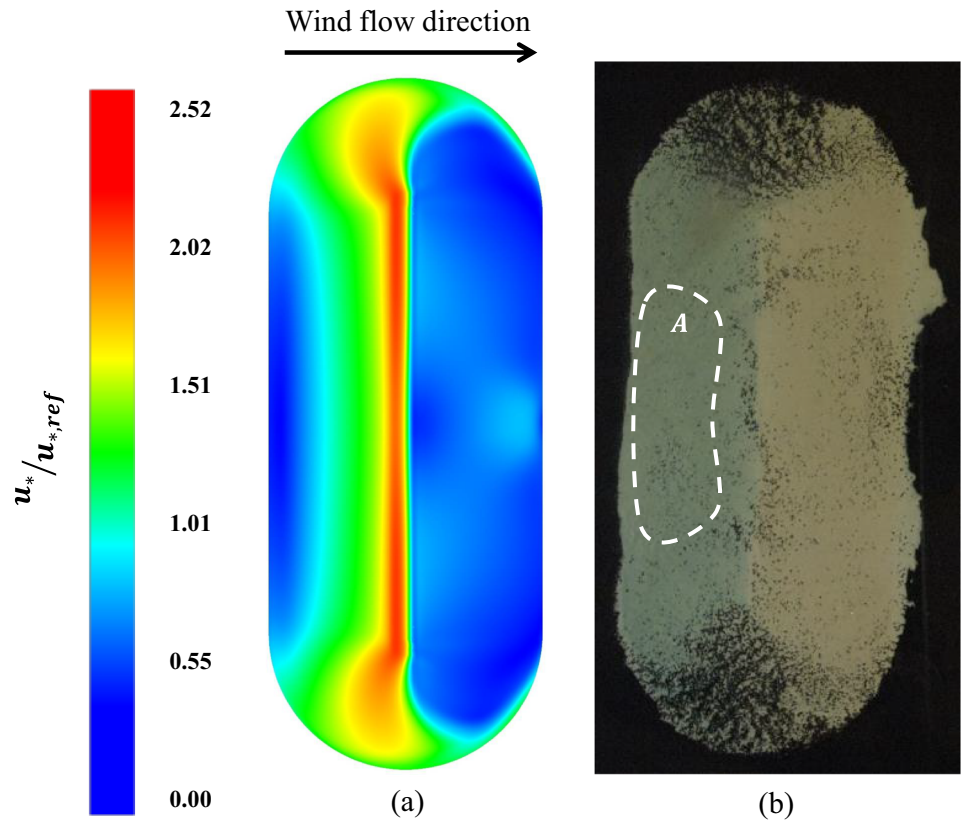


Fig. 8 Face-on cubic building case for $0.5 H_b$ and 7 m/s. **a** Difference between the friction velocity over the stockpile surface and the threshold friction velocity modified by the angle θ at which the fluid flows over the stockpile and **b** photograph of the top view of the eroded sand stockpile after pavement

Fig. 9 Temporal evolution of the erosion for a stockpile downstream a cubic building oriented 90° and 45° to the main flow, separated by gap of $0.5H_b$ for the upstream velocity of 8 m/s

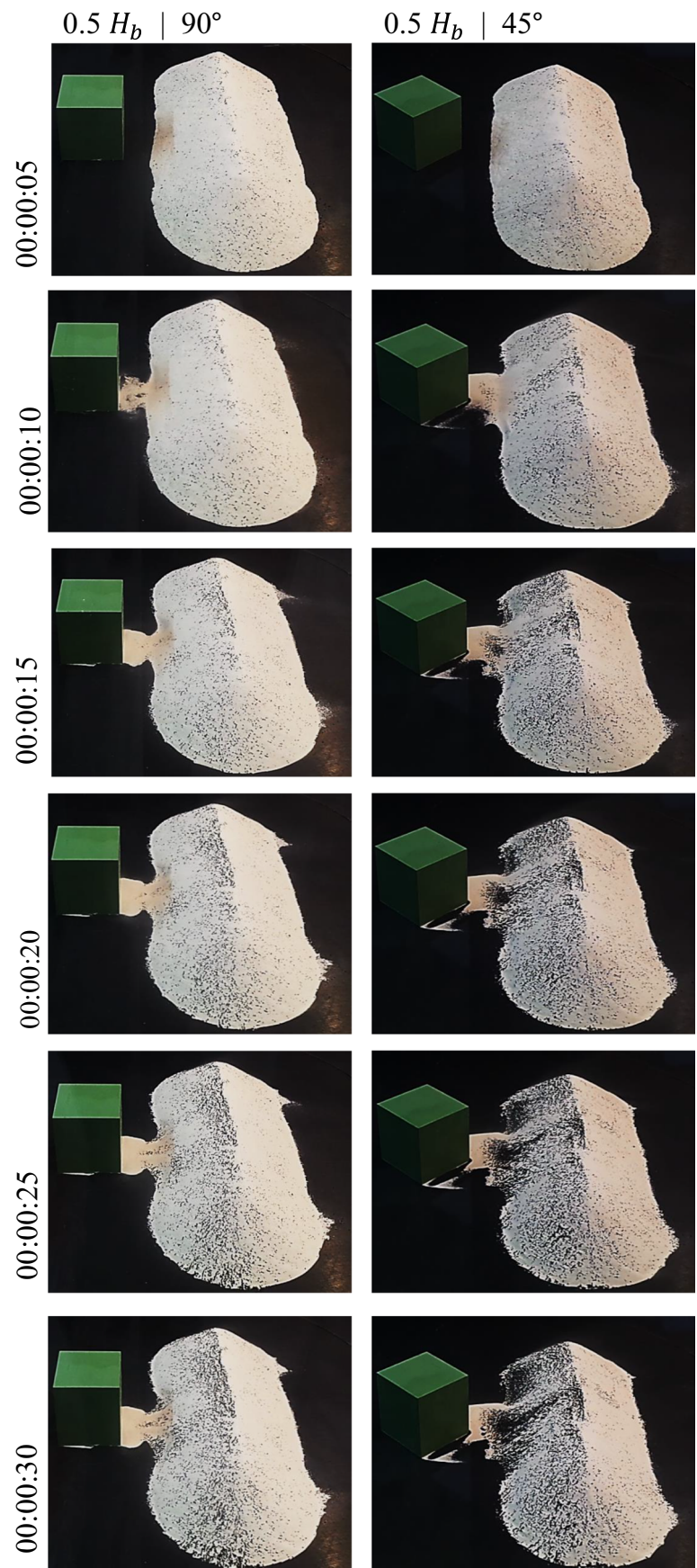


Fig. 10 Temporal evolution of the erosion for a stockpile downstream a cubic building oriented 45° to the main flow, separated by gaps of $0.5H_b$ and $1.5H_b$ for the upstream velocity of 8 m/s

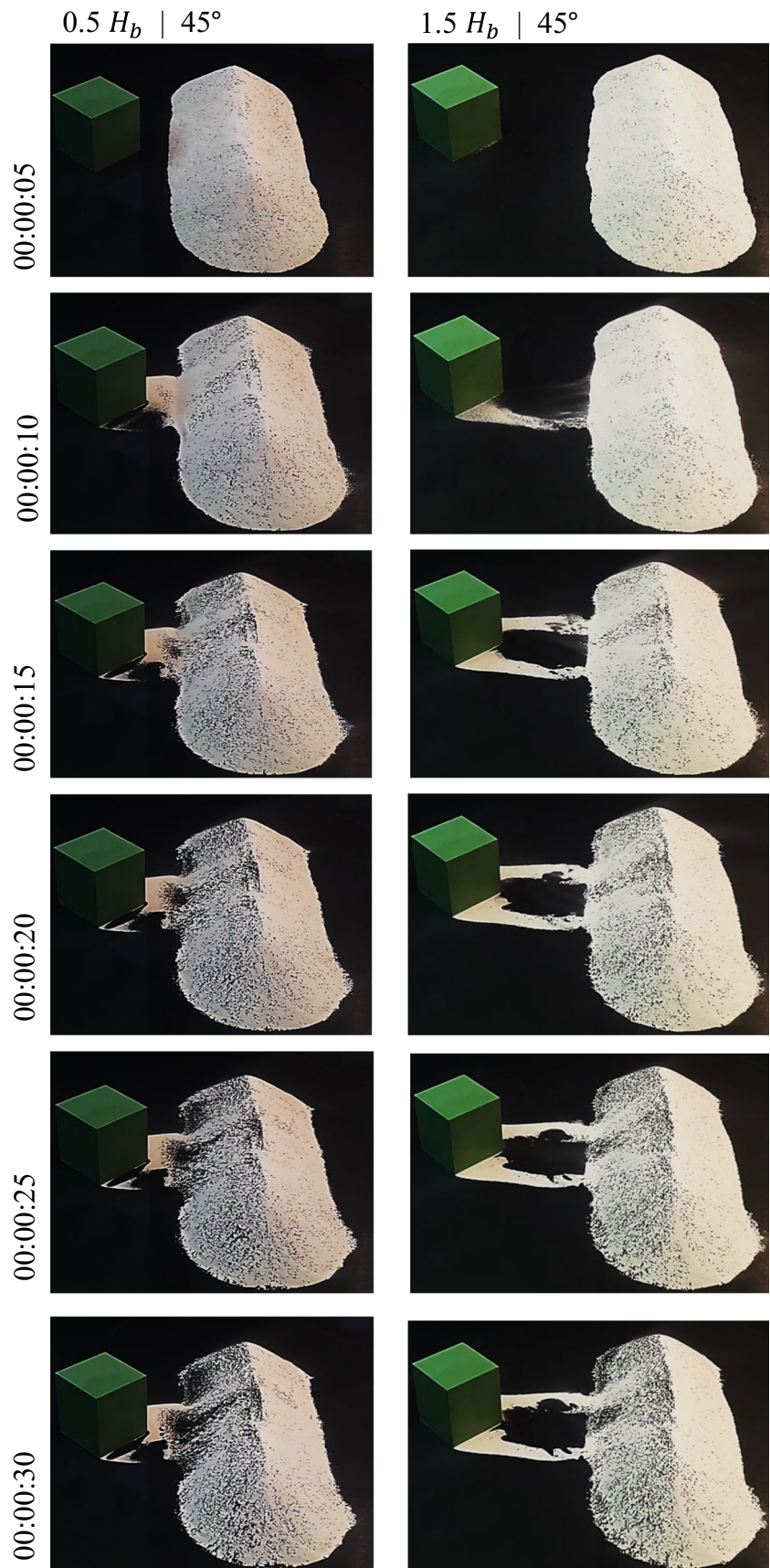


Table 1 Emitted mass (g) measurements from an isolated stockpile and from a stockpile downstream a cubic building with gaps $0.5H_b$ and $1.5H_b$ ($H_b = 10\text{ cm}$ is the building height)

U_∞ (m/s)	Isolated pile	Gap	Face-on	Edge-on
7	140.3 ± 8.4	$0.5H_b$	247.6 ± 14.9	282.7 ± 17.0
		$1.5H_b$	209.3 ± 12.6	319.5 ± 19.2
8	247.8 ± 14.9	$0.5H_b$	325.5 ± 19.5	413.0 ± 24.8
		$1.5H_b$	336.2 ± 20.2	452.5 ± 27.2
9	387.4 ± 23.2	$0.5H_b$	470.8 ± 28.2	518.5 ± 31.1
		$1.5H_b$	455.4 ± 27.3	542.4 ± 32.5

the erosion is much more significant downstream the cube. Figure 10 shows a more effective erosion when the gap is smaller. At shorter distances, the recirculation zone downwind the building directly interacts with the stockpile surface (also can be seen in Fig. 6c) leading to high levels of erosion evidenced again by the accumulation of non-erodible particles. For 9 m/s cases, the same analysis is valid.

Emitted mass measurements

Table 1 shows the emitted mass measurements from the wind tunnel experiments with an isolated stockpile and a stockpile downstream a cubic building. The results reveal that emissions considerably increase due to the presence of the building, that is, the isolated stockpile emits less than the pile downstream a cubic obstacle for all tested configurations. Furthermore, if the stockpile is downstream an edge-on cubic building, the impact is even stronger.

The increase of the gap distance between the building and the pile from $0.5H_b$ to $1.5H_b$ does not generate expressive changes in the emitted mass measurements in the 7 and 9 m/s cases, mainly if we take a look at the uncertainties. The differences between the emitted masses are very small. For cases at 8 m/s, the emitted mass slightly increased when the distance between the cubic building and the stockpile increased. The final analysis of the variation of the distance used in the present work can be considered inconclusive, since no well defined pattern was observed. However, as discussed above, the isolated stockpile, that is, a stockpile far enough from any obstacle, emits less in all tested cases. So, despite the inconclusive results about gaps, in industrial sites, it would be strategic to allocate the piles at a great distance from the buildings for precaution.

It is important to point out that there is an accumulation of sand on the ground between the cube and the pile for the tested cases. Therefore, the emitted mass can be higher than the estimated amount presented in Table 1 if the accumulated sand in the middle is considered.

Conclusion

Comparing the obtained experimental results with those for the isolated stockpile configuration and observing the differences in the erosion patterns and emission estimates was possible to conclude that (i) the emissions considerably increase due to the presence of the building, that is, the isolated stockpile emits less than the pile downstream a cubic obstacle for all tested configurations, mainly if the stockpile is downstream an edge-on cubic building; (ii) the higher the free stream velocity, due to the presence of the obstacle, the more efficient the dynamics of the pavement process is, that is, the vulnerable areas are covered more rapidly by the non-erodible particles (that create a protective effect); and (iii) the increase of the gap between the building and the pile from $0.5H_b$ to $1.5H_b$ does not generate expressive changes in the emitted mass measurements or follow some well-defined pattern. However, the analysis of the gaps reveals that smaller distances influence the particle distribution over the stockpile surface mainly downstream the cubic building showing areas where the erosion is more intense.

Despite the inconclusive results about the influence of the gaps in the emitted mass, in an industrial site, it would be strategic to allocate the pile at greater distances from buildings for precaution, since the isolated stockpile cases (stockpiles far enough from any building) showed smaller emitted masses. When avoiding buildings is not allowed, the recommendation is to allocate the stockpiles preferably downstream face-on buildings.

These findings play an important role since it is possible to obtain an optimal industrial open yard configuration where fewer particles are emitted to the atmosphere. In open yards where reallocation of buildings or industrial structures and sources is not possible, to understand how the wind erodes the sources is very relevant leading the site management to constitute a method of particulate control. Besides that, these results may be useful to improve

emission models since more detailed information about the friction velocity distribution in the sources was obtained.

Funding information This study was financed in part by the Coordenação de Aperfeiçoamento de Pessoal de Nível Superior - Brasil (CAPES) - Finance Code 001. It was also carried out with the financial support of Fundação de Amparo a Pesquisa e Inovação do Espírito Santo (FAPES) and Conselho Nacional de Desenvolvimento Científico e Tecnológico (CNPq).

References

- Aliabadi AA (2018) Theory and applications of turbulence. Amir A. Aliabadi Publications, p 181. isbn: 9780980970494
- Bachelet V, et al (2018) Elastic wave generated by granular impact on rough and erodible surfaces. In: Journal of Applied Physics 123(4). issn:10897550. <https://doi.org/10.1063/1.5012979>
- Badr T, Harion JL (2005) Numerical modelling of ow over stock-piles: implications on dust emissions. Atmos Environ 39(30):5576–5584. <https://doi.org/10.1016/j.atmosenv.2005.05.053>. issn: 13522310
- Badr T, Harion J-L (2007) Quantification of diffuse dust emissions from open air sources on industrial sites. In: 3rd IASME/WSEAS International Conference on Energy, Environment and Sustainable Development EEESD '07), ISBN: 978-960-8457-88-1 January, pp 276–280
- Bagnold RA (1941) An approach to the sediment transport problem from general physics. In: Physiographic and hydraulic studies of rivers
- Caliman MCFS (2017) Influence de particules dans le processus d'érosion éolienne. PhD thesis. Université de Rennes, p 144
- Chew LW, Aliabadi AA, Norford LK (2018) Flows across high aspect ratio street canyons: Reynolds number independence revisited. Environ Fluid Mech 18(5):1275–1291. <https://doi.org/10.1007/s10652-018-9601-0>. issn: 15731510
- Cong XC, Du HB et al (2013) Field measurements of shelter efficacy for installed wind fences in the open coal yard. J Wind Eng Ind Aerodyn 117:18–24. <https://doi.org/10.1016/j.jweia.2013.04.004>. issn: 01676105
- Cong XC, Yang GS et al (2016) Evaluating the dynamical characteristics of particle matter emissions in an open ore yard with industrial operation activities. Environ Sci Pollut Res 23(21):21336–21349. <https://doi.org/10.1007/s11356-016-7289-6>. issn: 16147499
- Cong XC, Yang SL et al (2012) Effect of aggregate stockpile configuration and layout on dust emissions in an open yard. Appl Math Model 36(11):5482–5491. <https://doi.org/10.1016/j.apm.2012.01.014>. issn: 0307904X
- Crawley DM, Nickling WG (2003) Drag partition for regularly arrayed rough surfaces. Boundary-Layer Meteorology 107(2):445–468. <https://doi.org/10.1023/A:1022119909546>. issn: 00068314
- Derakhshani SM, Schott DL, Lodewijks G (2013) Dust emission modelling around a stockpile by using computational fluid dynamics and discrete element method. AIP Conference Proceedings 1542:1055–1058. <https://doi.org/10.1063/1.4812116>. issn: 0094243X
- Diego I, et al (2009) Simultaneous CFD evaluation of wind flow and dust emission in open storage piles. Appl Math Model 33(7):3197–3207. <https://doi.org/10.1016/j.apm.2008.10.037>. issn: 0307904X
- Fang H et al (2018) An integrated simulation-assessment study for optimizing wind barrier design. Agric For Meteorol 263(August):198–206. <https://doi.org/10.1016/j.agrformet.2018.08.018>. issn: 01681923
- Faria R et al (2011) Wind tunnel and computational study of the stoss slope effect on the aeolian erosion of transverse sand dunes. Aeolian Research 3(3):303–314. <https://doi.org/10.1016/j.aeolia.2011.07.004>. issn: 18759637
- Farimani AB, Ferreira AD, Sousa ACM (2011) Computational modeling of the wind erosion on a sinusoidal pile using a moving boundary method. Geomorphology 130(3-4):299–311. <https://doi.org/10.1016/j.geomorph.2011.04.012>. issn: 0169555X
- Ferreira AD, Fino MRM (2012) A wind tunnel study of wind erosion and profile reshaping of transverse sand piles in tandem. Geomorphology 139-140:230–241. <https://doi.org/10.1016/j.geomorph.2011.10.024>. issn: 0169555X
- Ferreira AD, Pinheiro SR, Francisco SC (2013) Experimental and numerical study on the shear velocity distribution along one or two dunes in tandem. Environ Fluid Mech 13(6):557–570. <https://doi.org/10.1007/s10652-013-9282-7>. issn: 15677419
- Ferreira MCS, Furieri B, Ould El Moctar A et al (2019) A simple model to estimate emission of wind-blown particles from a granular bed in comparison to wind tunnel experiments. Geomorphology 335:1–13. <https://doi.org/10.1016/j.geomorph.2019.03.004>. issn: 0169555X
- Ferreira MCS, Furieri B, Santos JM et al (2019) An experimental and numerical study of the aeolian erosion of isolated and successive piles. In: Environmental Fluid Mechanics 0123456789. issn: 15731510. <https://doi.org/10.1007/s10652-019-09702-z>
- Foucaut JM, Stanislas M (1996) Take-off threshold velocity of solid particles lying under a turbulent boundary layer. Exp Fluids 20(5):377–382. <https://doi.org/10.1007/BF00191019>. issn: 07234864
- Funk R, Papke N, Hör B (2019) Wind tunnel tests to estimate PM10 and PM2.5-emissions from complex substrates of open cast strip mines in Germany. Aeolian Research 39(April):23–32. <https://doi.org/10.1016/j.aeolia.2019.03.003>. issn: 18759637
- Furieri B, Harion JL et al (2013) Numerical modelling of aeolian erosion over a surface with non-uniformly distributed roughness elements. Earth Surface Processes and Landforms 39(2):156–166. <https://doi.org/10.1002/esp.3435>. issn: 10969837
- Furieri B, Russeil S et al (2012a) Experimental surface flow visualization and numerical investigation of flow structure around an oblong stockpile. Environ Fluid Mech 12(6):533–553. <https://doi.org/10.1007/s10652-012-9249-0>. issn: 15677419
- Furieri B et al (2012b) Comparative analysis of dust emissions: isolated stockpile vs two nearby stockpiles. WIT Trans Ecology and The Environment 157:285–293. <https://doi.org/10.2495/AIR120>
- George KV et al (2017) Evaluation of coarse and fine particles in diverse Indian environments. Environmental Science and Pollution Research 24(4):3363–3374. <https://doi.org/10.1007/s11356-016-8049-3>. issn: 16147499
- Gillette DA, Stockton PH (1989) The effect of nonerodibles particles on wind erosion of erodible surfaces. Journal of Geophysical Research 94:12885–12893
- Gillies JA et al (2015) Using solid element roughness to control sand movement: Keeler Dunes, Keeler, California. Aeolian Research 18:35–46. <https://doi.org/10.1016/j.aeolia.2015.05.004>. issn: 18759637
- Giunta M (2020) Assessment of the environmental impact of road construction: modelling and prediction of fine particulate matter emissions. Building and Environment 176(March):106865. <https://doi.org/10.1016/j.buildenv.2020.106865>. issn: 03601323
- Harion J et al (2010) Improvement and validation of the method for quantification of fugitive dust emission on industrial sites. Tech. rep. Ecole des Mines de Douai , Centre ARMINES Douai, pp 1–70
- Hilton JE, Cleary PW (2013) Dust modelling using a combined CFD and discrete element formulation. Int J Numer in Fluids 72:528–549. <https://doi.org/10.1002/flid>

- Iversen JD, Rasmussen KR (1994) The effect of surface slope on saltation threshold. *Sedimentology* 41(4):721–728. <https://doi.org/10.1111/j.1365-3091.1994.tb01419.x>. issn: 13653091
- Iversen JD, Wang W et al (1990) The effect of a roughness element on local saltation transport. *Journal of Wind Engineering and Industrial Aerodynamics* 36:845–854
- Iversen JD, White BR (1982) Saltation threshold on Earth, Mars and Venus. *Sedimentology* 29:111–119
- Jeong CH et al (2014) Numerical investigation on influence of wind break wall height on dust scattering characteristics. *Journal of ILASS-Korea* 19(3):136–141. <https://doi.org/10.15435/jilasskr.2014.19.3.136>. issn: 1226-2277
- Kim RW et al (2017) Design of a windbreak fence to reduce fugitive dust in open areas. *Computers and Electronics in Agriculture* 149(August):150–165. <https://doi.org/10.1016/j.compag.2017.08.014>. issn: 01681699
- Leon Lyles RLS, Schmeidler NF (2013) How aerodynamic roughness elements control sand movement. *Transactions of the ASAE* 17(1):0134–0139. <https://doi.org/10.13031/2013.36805>
- Liu B, Qu J, Ning D (2018) Amplification factors to estimate wind erosion of piles of soil with different heights: numerical simulation and structure-from-motion photogrammetry verification. *Journal of Soil and Water Conservation* 73(4):377–385. <https://doi.org/10.2489/jswc.73.4.377>. issn: 19413300
- Liu H, Rodgers MO, Guensler R (2019) The impact of road grade on vehicle accelerations behavior, PM2.5 emissions, and dispersion modeling. *Transportation Research Part D: Transport and Environment* 75(September):297–319. issn: 13619209. <https://doi.org/10.1016/j.trd.2019.09.006>
- Marshall JK (1971) Drag measurements in roughness arrays of varying density and distribution. *Agricultural Meteorology* 8(C):269–292. issn: 00021571. [https://doi.org/10.1016/0002-1571\(71\)90116-6](https://doi.org/10.1016/0002-1571(71)90116-6)
- Martcorena B, Bergametti G (1995) Modeling the atmospheric dust cycle: 1. Design of a soil derived dust emission scheme.pdf.pdf. *Journal of Geophysical Research* 100:415–430
- Menter FR (1994) Two-equation eddy-viscosity turbulence models for engineering applications. *AIAA Journal* 32(8):1598–1605. issn: 0001-1452. <https://doi.org/10.2514/3.12149>. <http://arc.aiaa.org/doi/10.2514/3.12149>,
- Miri A, Dragovich D, Dong Z (2017) Vegetation morphologic and aerodynamic characteristics reduce aeolian erosion. *Sci Rep* 7(1):1–9. <https://doi.org/10.1038/s41598-017-54313-0>. issn: 20452322
- de Moraes CL et al (2018) Influence of non-erodible particles with multimodal size distribution on aeolian erosion of storage piles of granular materials. *Environmental Fluid Mechanics* 0123456789. issn: 15731510. <https://doi.org/10.1007/s10652-018-9640-6>
- Novak L et al (2015) Numerical modeling of dust lifting from a complex-geometry industrial stockpile. *Strojnicki Vestnik/Journal of Mechanical Engineering* 61(11):621–631. <https://doi.org/10.5545/sv-jme.2015.2824>. issn: 00392480
- Raupach MR (1992) Drag and drag partitioning on rough surfaces. *Boundary-Layer Meteorology* 60:375–395
- Raupach R et al (1993) The effect of roughness elements on wind erosion threshold. In: 98(92): 3023–3029
- Romeo A et al (2017) Dust emission and dispersion from mineral storage piles. *Environmental Science and Pollution Research* 24(28):22663–22672. <https://doi.org/10.1007/s11356-017-9881-9>. issn: 16147499
- Shao Y (2008) *Physics and modelling of wind erosion*, 2nd edn. Springer, Berlin, p 459
- Shao Y, Lu H (2000) A simple expression for wind erosion threshold friction velocity. *Journal of Geophysical Research* 105:437–443
- Tan L et al (2013) Aeolian sand transport over gobi with different gravel coverages under limited sand supply: a mobile wind tunnel investigation. *Aeolian Research* 11:67–74. issn: 18759637. <https://doi.org/10.1016/j.aeolia.2013.10.003>
- Toraño JA et al (2007) Influence of the pile shape on wind erosion CFD emission simulation. *Applied Mathematical Modelling* 31(11):2487–2502. <https://doi.org/10.1016/j.apm.2006.10.012>. issn: 0307904X
- Turpin CTB, Harion JL (2010) Numerical modelling of aeolian erosion over rough surfaces. *Earth Surface Processes and Landforms* 35(12):1418–1429. issn: 10969837. <https://doi.org/10.1002/esp.1980>
- Turpin C, Harion JL (2009) Numerical modeling of flow structures over various at-topped stockpiles height: implications on dust emissions. *Atmos Environ* 43(35):5579–5587. issn: 13522310. <https://doi.org/10.1016/j.atmosenv.2009.07.047>
- Turpin C, Harion JL (2010) Effect of the topography of an industrial site on dust emissions from open storage yards. *Environmental Fluid Mechanics* 10(6):677–690. <https://doi.org/10.1007/s10652-010-9170-3>. issn: 15677419
- Turpin C (2010) Amélioration des modèles de quantification des émissions particulaires diffuses liées à l'érosion éolienne de tas de stockage de matières granulaires sur sites industriels. PhD thesis. Université de Valenciennes et du Hainaut Cambrésis, p 239
- USEPA (2006) 13.2.5 Industrial wind erosion. In: *Compil Air Pollut Emiss Factors 1*. [https://doi.org/10.1130/0091-7613\(1998\)026\(0363](https://doi.org/10.1130/0091-7613(1998)026(0363)
- Walter B, Voegeli C, Horender S (2016) Estimating sediment mass fluxes on surfaces sheltered by live vegetation. *Boundary-Layer Meteorology* 163(2):273–286. <https://doi.org/10.1007/s10546-016-0224-z>. issn: 15731472
- White BR (1996) Laboratory simulation of aeolian sand transport and physical modelling. *Annals of Arid Zone* 35(3):187–213
- Woodruff NP, Zingg AW (1953) Wind tunnel studies of shelter belt models. *J Forestry* 51:173

Publisher's note Springer Nature remains neutral with regard to jurisdictional claims in published maps and institutional affiliations.